Thermal Expansion in $BaRuO_3$ Perovskites – an unusual case of bond strengthening at high temperatures

Paula Kayser, Sean Injac, Brendan J. Kennedy* and Andre L. Menezes de Oliveira

School of Chemistry, The University of Sydney, Sydney, NSW 2006, Australia

Yuichi Shirako and Masashi Hasegawa

Department of Crystalline Materials Science, Nagoya University, Furo-cho, Chikusa-ku, Nagoya 464-8603 Japan

Abstract

The temperature dependence of the structures of three polytypes of $BaRuO_3$ have been investigated between room temperature and 1000 °C using high resolution Synchrotron X-ray diffraction. The structural studies reveal a systematic decrease in the Ru-Ru distance as the pressure required to prepare the polytype increases. The O-O distance across the shared face increases as the Ru-Ru separation decreases. The 9*R* and 4*H* polytypes undergo unexceptional changes with increasing temperature. In 6*H*-$BaRuO_3$ there is an apparent increase in the Ru-Ru interaction around 650 °C and concurrent reduction in the O-O distance indicating an anomalous strengthening of the Ru-Ru interactions upon heating.

Keywords: Thermal Expansion; Perovskite; face sharing perovskites; $BaRuO_3$

Introduction

Perovskites are probably the most commonly encountered metal oxide structural type, and arguably amongst the most technologically important. Interest in perovskite oxides stems not only from their importance in geology, $CaSiO_3$ perovskite is one of the major constituent minerals in the deep Earth[1], but also because of the diverse array of electronic and magnetic properties perovskites display. Perovskites containing a second row transition metal provide multiple examples of interesting electronic and magnetic properties: Sr_2RuO_4 displays unconventional p-wave superconductivity [2], $Sr_3Ru_2O_7$ exhibits metallic metamagentic behaviour [3], $SrRuO_3$ is a metallic ferromagnetic [4] and $SrTcO_3$ is an antiferromagnetic with an extraordinary high Neel temperature [5]. The temperature dependence of perovskite structures are of interest from both a fundamental viewpoint of understanding crystallographic phase transitions [6,7], and unusual phenomena such as Negative Thermal Expansion [8,9] as well as for practical applications including in solid oxide fuel cells [10,11] and nuclear waste immobilisation [12].

The precise structure of the A*B*O_3 perovskites is dependent on the relative size of the cations, often described by the tolerance factor $t = \frac{(r_A + r_O)}{\sqrt{2}(r_B + r_O)}$, where r_A, r_B, and r_O correspond to the radius of the *A* and *B* site cations and the oxygen anions respectively, synthetic conditions and the electronic configuration of the cations. Both $CaRuO_3$ and $SrRuO_3$ have $t < 1$ and the oxides adopt an orthorhombic structure based on corner sharing RuO_6 octahedra at room temperature. $BaRuO_3$ has $t > 1$ and, when synthesised at ambient pressure, adopts a rhombohedral structure containing a mixture of face shared and corner shared RuO_6 octahedra. The face-sharing versus corner sharing connections of the RuO_6 octahedra correspond to hexagonal (*h*) close packing versus cubic (*c*) close packing of the BaO_3 layers in the perovskite structure. Rhombohedral $BaRuO_3$ has a 9*R* polytype structure with a *hhchhchhc* stacking sequence. Three other polymorphs of $BaRuO_3$ have been isolated from high pressure synthesis, namely the 4*H* (*hchc*), 6*H*(*cchcch*) and 3*C* (*ccc*) structures where the percentage of corner shared connectivity increases from 33%, 50%, 66% to 100% for the 9*R*, 4*H*, 6*H* and 3*C* phases respectively with the pressure required to prepare the last three phases being 3 GPa, 5GPa and 18 GPa [13]. $SrMnO_3$ undergoes a thermally induced 6*H*→ 3*C* transformation around 1035 °C at ambient pressure [14].

The four $BaRuO_3$ polymorphs have different electronic and magnetic properties[15-17]. The 9*R* and 4*H*-$BaRuO_3$ compounds are paramagnetic, 6*H*-$BaRuO_3$ is on the verge of

ferromagnetic order and 3*C*-$BaRuO_3$ is ferromagnetic. The presence of the strong Ru-Ru metal bonding along the *c*-axis in rhombohedral and hexagonal $BaRuO_3$ gives one-dimensional (1D) character and it has been suggested that a pseudogap in the band structure of 9*R*-$BaRuO_3$ opens near the metal-insulator transition due to the presence of charge density wave (CDW) fluctuations [16,18]. High pressure diffraction and Raman spectroscopy studies of 9*R*-$BaRuO_3$, at ambient temperature, have revealed an anomalous increase in the Ru-Ru distance hinting at an electronic topological transition [19].

In comparison to the corner sharing perovskites such as $CaTiO_3$ [7] and $SrRuO_3$ [20] there is a scarcity of high temperature structural studies of hexagonal perovskites, in particular of those containing 4d or 4d transition metals. In hexagonal perovskites such as $BaRuO_3$ the RuO_6 octahedra are face-shared, leading to a shorter Ru-Ru distance than in Ru metal. This indicates a stronger hybridization of the Ru 4d orbitals and the resulting molecular orbital formation may introduce an additional internal charge degree of freedom. The aim of the present work is to establish accurate and precise temperature dependent structures for the three hexagonal polymorphs of $BaRuO_3$ in order to enhance understanding of the M-M interactions in hexagonal perovskites.

Experimental

Synthesis: The ambient pressure sample, 9*R*-$BaRuO_3$, was prepared using conventional solid state synthesis. Stoichiometric amounts of $BaCO_3$ and RuO_2 were ground in an acetone slurry employing an agate mortar and pestle. The powder was pressed into a pellet and heated at 900 ºC for 12 h. The high-pressure phases were obtained using a cubic anvil press. The powder sample was placed in a Pt foil container and loaded into a cylindrical BN capsule located at the centre of the cube. A thin, rolled, Mo foil was used as the heater. This was placed in a semi-dried pyrophyllite cube as a pressure medium. Pyrophyllite plugs and Mo disks, that act as electrodes, were placed at both ends of the Mo heater. The sample was kept at 2 GPa or 6 GPa and 900 ºC for 30 min to synthesize 4*H*- or 6*H*-$BaRuO_3$, respectively. Thermogravimetric analysis (TGA) of the complexes was carried out using a TA Instruments Discovery TGA. Measurements were conducted with a heating rate of 5°/min under an air atmosphere.

Structure Determination: Synchrotron X-ray powder diffraction (S-XRD) data were collected using the powder diffractometer at beamline BL-10 of the Australian Synchrotron

[21]. The samples were finely ground and housed in sealed 0.2 mm diameter quartz capillaries that were rotated during the measurements to improve powder averaging and to reduce the effects of preferred orientation. The wavelength was set at ~ 0.775 Å, and the precise value of this was determined using a NIST LaB_6 standard reference material. Data were collected from RT to 1270 K using a Cyberstar hot-air blower. The structures described here were refined by the Rietveld method as implemented in the program GSAS/EXPGUI [22,23]. The peak shapes were modelled using a pseudo-Voigt function and the background was estimated using a shifted Chebyschev function. The scale factor, detector zero point, lattice parameters, atomic coordinates and atomic displacement parameters were refined together with the peak profile parameters. All sites were assumed to be fully occupied and there is no evidence from the refinements for any Ba-Ru anti-site disorder. The atomic displacement parameters of the independent anions were constrained to be equal.

Results and Discussion

Samples of the 9*R*, 4*H* and 6*H* polymorphs of $BaRuO_3$ were prepared by established methods and the quality and purity of the samples was verified by Synchrotron X-ray Diffraction (S-XRD) measurements. The structures of the samples were refined against the S-XRD data using the Rietveld method, and examples of these are given in Figures 1. The positional and thermal parameters for the three polymorphs of $BaRuO_3$ studied in the present work are given in Table 1, and selected interatomic distances are in Table 2. The crystal structures of the four $BaRuO_3$ polymorphs are represented in Figure 2.

The 9*R* polytype of $BaRuO_3$ is formed at ambient pressure. It has a rhombohedral structure with space group $R\bar{3}m$ and lattice parameters in the hexagonal cell are a = 5.74823(20) and c = 21.5783(8) Å. The current refined atomic coordinates for O(1); x = 0.1679(4), z = 0.10798(20) in 9*R*-$BaRuO_3$ are in excellent agreement with the values obtained from an earlier powder neutron diffraction study by Santoro *et al.* (x = 0.1769, z = 0.1082) [24]. This gives a high degree of confidence in the refined structures. The ability to refine accurate and precise structures from the S-XRD data, despite the presence of heavy Ba and Ru cations, reflects both the quality of the data and the relatively small number of variable positional parameters associated with the light oxygen anions in each of the structures.

In the 9*R* structure, three RuO_6 octahedra share faces forming a Ru_3O_{12} trimer, with a Ru-Ru separation across the shared face of 2.523(1) Å. There is a strong Ru-Ru interaction

across the shared face and the shortness of this distance has been taken as evidence for the formation of a Ru-Ru bond [25 26]. The Ru_3O_{12} trimers are connected by corner sharing giving a *hhchhchhc* stacking sequence, see Figure 2. The O(1) and O(2) atoms occupy the corner sharing and face sharing positions respectively. The O(2)-O(2) distance across the shared face, 2.698(3) Å, is shorter than the O(1)-O(1) distance of 2.8741(2) Å. This is a common feature of the 9*R*-type perovskites; for example in 9*R*- $BaSiO_3$ the Si-Si distance is 2.509 Å (*cf* the Si-Si distance in elemental Si of 2.34 Å) and the corresponding O-O distances are O(2)-O(2) 2.252 and O(1)-O(1) 2.650 Å [27].

Increasing the pressure of synthesis increases the number of corner connects and results in a reconstructive phase transition to the hexagonal 4*H*-$BaRuO_3$ structure in space group $P6_3/mmc$. The lattice parameters obtained from refinement against the S-XRD data recorded at room temperature were a = 5.731782(2) Å and c = 9.506246(33) Å. The 4*H* structure contains pairs of face sharing RuO_6 octahedra that form Ru_2O_9 dimers[26], with a short Ru-Ru bond of 2.54067(7) Å. The dimers are connected by corner sharing of the octahedra to give a *hchc* stacking sequence, Figure 2. As seen for the 9*R* polytype the O(2)-O(2) distance across the shared face 2.642(4) is shorter than the corner sharing O(1)-O(1) distance of 2.8659(1) Å. Further increasing the pressure of synthesis to 6 GPa resulted in the formation of a second hexagonal structure 6*H*-$BaRuO_3$ [28], also described in space group $P6_3/mmc$, that also contains Ru_2O_9 dimers [29]. In the 6*H* structure the Ru_2O_9 dimers corner share with RuO_6 octahedra giving a *cchcch* stacking sequence, Figure 2. The lattice parameters obtained from refinement against the S-XRD data recorded at room temperature are a = 5.71590(6) Å and c = 14.05664(15) Å. The Ru-Ru bond length in the Ru_2O_9 dimers is 2.5626(11) Å and the O(2)-O(2) distance across the shared face of 2.616(4) is shorter than the O(1)-O(1) distance of 2.916(1) Å. The average Ru-O distances in each of the octahedral units of the three polymorphs fall within a narrow range (1.971-2.007 Å) and are typical of tetravalent ruthenium oxides such as RuO_2 and $SrRuO_3$ [20,30]. This is supported by Bond Valence Sum calculations. The BVS for the Ru sites in 9*R*-$BaRuO_3$ are 3.76 and 3.95 for Ru(1) and Ru(2) respectively, in 4*H*-$BaRuO_3$ it is 3.96 and in 6*H*-$BaRuO_3$ the values for Ru(1) is 4.14 and for Ru(2) it is 3.86. Values for the Ba cations and anions are given in Table 1. The powder diffraction data provided no indication for structural modulations observed in 9*R*-$BaRuO_3$ at low temperatures.[31]

Comparing the three room temperature structures it is observed that that Ru-Ru bond distance increases across the series 9*R* – 4*H* – 6*H*. For each of these oxides the Ru-Ru

contact across the shared face is less than the shortest contact in ruthenium metal (2.65 Å). This is indicative of strong orbital overlap between ruthenium cations within the Ru-O octahedral oligomer [32]. Similar short distances have been observed in structurally related oxides including 2.56 Å in $Ba_4Ru_3O_{10}$ which has a trimer arrangement [33], and 2.57 Å across the RuO_6 dimers in Li_2RuO_3 [34]. This increase is related to a decrease in the O(2)-O(2) distance across the shared face and a concurrent increase in the O(1)-O(1) distance from 2.8659(1) in the 4H structure and 2.874(2) Å in the 9*R* structure to 2.916(1) Å in the 6*H* structure. Santoro *et al.* have suggested that the relatively short non-bonding O(2)-O(2) distance acts to minimise the Ru-Ru repulsion across the faces [24]. That the Ru-Ru distance does not systematically decrease as O(2)-O(2) distance increases, indicates that factors other than the electrostatic repulsion of the cations play a role [35,36]. There is strong electrostatic repulsion between the Ru cations in the face sharing octahedra. This is minimised by displacement of the cation from the centre of the octahedra and away from the shared face. A similar displacement is observed in $BaTiO_3$ and $SrMnO_3$ that also adopt 6*H* type structures where the *M*-*M* distance is 2.690(4) Å in $BaTiO_3$ [29] and 2.511(2) Å in $SrMnO_3$ [37] and in the 4*H* polymorph of $SrMnO_3$ where the Mn-Mn distance is 2.500(6) Å [38]. The relatively short O-O separation across the shared face is consistent with the suggestion of Santoro *et al.* that this acts to reduce the *M*-*M* repulsion [24]. Sondena *et al.* [39] have shown that displacement of the Mn cation in $AMnO_3$ promotes charge transfer between the Mn and O resulting in a lower charge on the oxygen atoms on the oxygen triangle of the shared face compared to those oxygen anions in the plane where the octahedra share corners. This results in a contraction of the oxygen triangle that shields the repulsive interaction. It is likely that covalent bonding between the Ru and O plays a role in optimising the geometry of the shared oxygen face.

Taking the Ru-Ru distance as a proxy for the bond strength, it appears that this decreases as the pressure required to prepare the polytype increases; that is 6*H*-$BaRuO_3$ has the weakest attractive interaction. Likewise the DFT calculations of Sondena *et al.* [39] suggest it is possible to use the O(2)-O(2) distance across the shared face as a proxy for shielding of the repulsion between the Ru cations, and the changes in this suggest the shielding is most significant in 6*H*-$BaRuO_3$ despite this having the longest Ru-Ru separation and presumably the weakest attraction.

The temperature dependence of the unit cell parameters, cell volume and the Ru-Ru distance for each of the three $BaRuO_3$ samples are illustrated in Figures 3-5. Although the 4*H* polytype is obtained from quenching from High Pressure-Temperature conditions it was

observed to be stable to heating to 1000 °C. .The diffraction pattern of the sample cooled to 100 °C after heating to 1000 °C was essentially identical to that observed in the initial heating cycle. The thermal expansion of the 9*R* and 4*H* samples are unexceptional, both showing conventional positive thermal expansion. TGA measurements revealed no significant weight change on heating either sample to 950 °C under an air atmosphere (see supplementary information (SI)). In general the Atomic Displacement Parameters (ADPs) and Ru-Ru distance show systematic increases upon heating, Figure 3 and 4, although this is clearly non-linear for the Ru cations in the 9*R* polytype. The results for the 6*H* sample are more interesting. Firstly we observed the sample to be somewhat unstable upon heating to above 800 °C, with a number of unindexed peaks (they are not due to the 9*R* polytype) appearing in the profile, however the rate of decomposition was sufficiently slow, even at the highest temperature investigated, that an acceptable refinement could be obtained; R_p increased from 3.80 at 25 °C to 5.08 at 1000 °C. That the unindexed peaks persisted upon cooling the sample to room temperature (see SI) demonstrates that changes above 800 °C are due to decomposition and not a transition to another structure. This was substantiated by the TGA measurements that showed a small weight gain above 800 °C. The thermal expansion of the unit cell parameters and cell volume of the 6*H* sample is similar to that displayed by the 9*R* and 4*H* structures. The major difference is in the Ru-Ru distance that initially increases before reaching a plateau near 650 °C, well below the temperature where sample decomposition occurs, as demonstrated by both the XRD and TGA measurements. In comparison the Ru(1)-Ru(2) distance across the shared corners shows an approximately linear increase as the temperature is increased for all three oxides, see Figure 6.

Included in Figures 3-5 are the temperature dependence of the full width at half maximum (FWHM) of selected low angle peaks. For the 9*R* and 4*H* samples these remained essentially constant as the sample was heated, whereas for the 4*H* sample the width of the 103 reflection, near $2\theta = 13°$, begins to increase around 800 °C, that is near where the first unindexed peaks appeared in the diffraction patterns. Critically this, and other reflections, did not broaden near 650 °C, the temperature where the Ru-Ru thermal expansion plateaus. There is a rapid increase in the ADPs of the various atoms, but most particularly the oxygen anions above 800 °C. Finally we note there is a change in the Ru(2)-O distances around 650 °C, see SI.

The thermal expansion behaviour of the $BaRuO_3$ samples is compared in Figure 7 and the linear thermal expansion coefficients (TEC) between 50 and 600 °C , defined as $\alpha_i =$

$\frac{(a_{600}-a_{50})}{a_{50}*\Delta T}$ where *i* is the unit cell direction and ΔT the change in temperature, are given in Table 3. The average linear TEC $\bar{\alpha}$ was calculated in a similar manner using the cube root of the volume. There is a slight reduction in the thermal expansion coefficients in the higher temperature region, which may be indicative of a small change in the oxygen stoichiometry of the sample, although the TGA measurements for the 9*R* and 4*H* did not reveal any significant change. The values of the TEC for the three polymorphs are all similar and exhibit slight anisotropy with $\alpha_c < \alpha_a$. The average TEC values are similar to those seen in the layered perovskite $NdBaInO_4$ $\bar{\alpha}$ =11.8 K^{-1} [40] and other perovskite type materials[41].

The S-XRD studies demonstrate that none of the $BaRuO_3$ samples undergo a thermally induced structural transition between RT and 1000 °C. However, Figure 5 reveals an anomalous change in the Ru-Ru distances in 6*H*-$BaRuO_3$ around 650 °C. Examination of the impact of temperature on the O-O contacts within the face sharing units, Figure 8, is illustrative. The longer O(1)-O(1) distance is equal to *a*/2 in both the 9*R* and 4*H* structures and displays a systematic increase with temperature. In the 6*H* structure the O(1)-O(1) distance is dependent on both the unit cell *a*-parameter and the *x*-coordinate of the O(1) anion, given by $d = a * (3 - x_{O1})$. This shows a systematic increase upon heating to 600 °C and then it begins to decrease. The O(2)-O(2) distance in the 9*R*-$BaRuO_3$ (=$a * (1 - x_{O2})$) and 4*H*-$BaRuO_3$ (=$a * (1 - \frac{3}{2}x_{O2})$) are essentially independent of temperature while the corresponding distance in the 6*H* structure (given by $a * (2 - 3x_{O2})$) appears to decrease more rapidly above 600°C.

Evidently the change in the Ru-Ru distances in 6*H*-$BaRuO_3$ around 650 °C is associated with a change in the displacement of the oxygen atoms at the shared face. The linking of the Ru_2O_9 units to neighbouring octahedra by corner, rather than face sharing, facilitates the displacement of the Ru cations within the dimer units from the centre of the octahedra and away from the shared face, thus reducing electrostatic repulsion between them. This is accompanied by a compression in the oxygen triangle in the shared face that acts to shield the cations. Sodena *et al.* [39] have argued that the compression of the oxygen triangle is facilitated by covalency that reduces the charge on the oxygen atoms in the face sharing triangles.

As noted above the Ru-Ru distance can be considered as a measure of the attractive Ru-Ru interactions. Surprisingly in 6*H*-$BaRuO_3$ there is an apparent increase in the Ru-Ru interaction around 650 °C that negates the temperature induced lengthening of the Ru-Ru

distances. That is there is an increase in the strength of these interactions. Following the arguments of Sodena *et al.* [39] this strengthening of the Ru-Ru attractive forces is aided by increased shielding of the shared face evident in the reduced O(2)-O(2) distance. The changes observed in the Ru-Ru and O-O separations in 6*H*-$BaRuO_3$ at high temperature suggests a strengthening of the Ru-Ru interactions occurs. Mandal *et al.*[19] have observed a similar anomaly in 9*R*-$BaRuO_3$ at high pressure and suggested is a result of an electronic topological transition associated the interactions of the 1-D molecular orbital like states with the conduction electrons. It is likely that a similar effect is happening here. We offer no explanation for why this occurs in the 6*H* polytype and not the other two polytypes.

Acknowledgments

This work was, in part, performed at the powder diffraction beamline at the Australian Synchrotron with the assistance of Dr Helen Brand. BJK acknowledges the support of the Australian Research Council. André Menezes would like to thank the CNPq (Process 232680/2014-0) for his postdoctoral fellowship.

References

(1) Mao, H. K.; Chen, L. C.; Hemley, R. J.; Jephcoat, A. P.; Wu, Y.; Bassett, W. A. *Journal of Geophysical Research-Solid Earth and Planets* **1989**, *94*, 17889.
(2) Maeno, Y.; Hashimoto, H.; Yoshida, K.; Nishizaki, S.; Fujita, T.; Bednorz, J. G.; Lichtenberg, F. *Nature* **1994**, *372*, 532.
(3) Borzi, R. A.; Grigera, S. A.; Farrell, J.; Perry, R. S.; Lister, S. J. S.; Lee, S. L.; Tennant, D. A.; Maeno, Y.; Mackenzie, A. P. *Science* **2007**, *315*, 214.
(4) Longo, J. M.; Raccah, P. M.; Goodenough, J. B. *Journal of Applied Physics* **1968**, *39*, 1327.
(5) Rodriguez, E. E.; Poineau, F.; Llobet, A.; Kennedy, B. J.; Avdeev, M.; Thorogood, G. J.; Carter, M. L.; Seshadri, R.; Singh, D. J.; Cheetham, A. K. *Physical Review Letters* **2011**, *106*, 067201.
(6) Howard, C. J.; Knight, K. S.; Kennedy, B. J.; Kisi, E. H. *Journal of Physics-Condensed Matter* **2000**, *12*, L677.
(7) Kennedy, B. J.; Howard, C. J.; Chakoumakos, B. C. *Journal of Physics-Condensed Matter* **1999**, *11*, 1479.
(8) Takenaka, K.; Takagi, H. *Applied Physics Letters* **2005**, *87*, 261902.
(9) Yamada, I.; Tsuchida, K.; Ohgushi, K.; Hayashi, N.; Kim, J.; Tsuji, N.; Takahashi, R.; Matsushita, M.; Nishiyama, N.; Inoue, T.; Irifune, T.; Kato, K.; Takata, M.; Takano, M. *Angewandte Chemie-International Edition* **2011**, *50*, 6579.
(10) Vente, J. F.; Haije, W. G.; Rak, Z. S. *Journal of Membrane Science* **2006**, *276*, 178.
(11) Jacobson, A. J. *Chemistry of Materials* **2010**, *22*, 660.
(12) Lumpkin, G. R. *Elements* **2006**, *2*, 365.
(13) Jin, C. Q.; Zhou, J. S.; Goodenough, J. B.; Liu, Q. Q.; Zhao, J. G.; Yang, L. X.; Yu, Y.; Yu, R. C.; Katsura, T.; Shatskiy, A.; Ito, E. *Proceedings of the National Academy of Sciences of the United States of America* **2008**, *105*, 7115.
(14) Rormark, L.; Morch, A. B.; Wiik, K.; Stolen, S.; Grande, T. *Chemistry of Materials* **2001**, *13*, 4005.

(15) Kanungo, S.; Datta, R.; Panda, S. K.; Saha-Dasgupta, T. *Journal of Physics-Condensed Matter* **2013**, *25*.
(16) Lee, Y. S.; Lee, J. S.; Kim, K. W.; Noh, T. W.; Yu, J. J.; Bang, Y.; Lee, M. K.; Eom, C. B. *Physical Review B* **2001**, *64*, 165109.
(17) Felser, C.; Cava, R. J. *Physical Review B* **2000**, *61*, 10005.
(18) Lee, Y. S.; Noh, T. W.; Park, J. H.; Lee, K. B.; Cao, G.; Crow, J. E.; Lee, M. K.; Eom, C. B.; Oh, E. J.; Yang, I. S. *Physical Review B* **2002**, *65*, 235113.
(19) Mandal, G.; Basu, A.; Mukherjee, G. D. *Materials Research Express* **2014**, *1*, 035700.
(20) Kennedy, B. J.; Hunter, B. A. *Physical Review B* **1998**, *58*, 653.
(21) Wallwork, K. S.; Kennedy, B. J.; Wang, D. *AIP Conference Proceedings* **2007**, *879*, 879.
(22) Larson, R. B.; Von Dreele, R. B. *General Structure Analysis System (GSAS)*, Los Alamos National Laboratory, 1994.
(23) Toby, B. H. *Journal of Applied Crystallography* **2001**, *34*, 210.
(24) Santoro, A.; Natali Sora, I.; Huang, Q. *Journal of Solid State Chemistry* **2000**, *151*, 245.
(25) Kauffmann, M.; Roussel, P.; Abraham, F. *Journal of Solid State Chemistry* **2007**, *180*, 1957.
(26) Hong, S. T.; Sleight, A. W. *Journal of Solid State Chemistry* **1997**, *128*, 251.
(27) Yusa, H.; Sata, N.; Ohishi, Y. *American Mineralogist* **2007**, *92*, 648.
(28) Longo, J. M.; Kafalas, J. A. *Materials Research Bulletin* **1968**, *3*, 687.
(29) Zhao, J. G.; Yang, L.; Yu, Y.; Li, F. Y.; Yu, R. C.; Fang, Z.; Chen, L. C.; Jin, C. Q. *Journal of Solid State Chemistry* **2007**, *180*, 2816.
(30) Bolzan, A. A.; Fong, C.; Kennedy, B. J.; Howard, C. J. *Acta Crystallographica Section B-Structural Science* **1997**, *53*, 373.
(31) Du, C. H.; Yao, C. H.; Ling, D. C.; Tang, M. T.; Hsu, F. C.; Liu, H. L.; Hatton, P. D.; Ikeda, N. *Journal of Physics-Condensed Matter* **2010**, *22*, 5.
(32) Streltsov, S. V.; Khomskii, D. I. *Physical Review B* **2012**, *86*, 064429.
(33) Igarashi, T.; Nogami, Y.; Klein, Y.; Rousse, G.; Okazaki, R.; Taniguchi, H.; Yasui, Y.; Terasaki, I. *Journal of the Physical Society of Japan* **2013**, *82*, 6.
(34) Miura, Y.; Yasui, Y.; Sato, M.; Igawa, N.; Kakurai, K. *Journal of the Physical Society of Japan* **2007**, *76*, 4.
(35) Stitzer, K. E.; Smith, M. D.; Gemmill, W. R.; zur Loye, H.-C. *Journal of the American Chemical Society* **2002**, *124*, 13877.
(36) Kimber, S. A. J.; Senn, M. S.; Fratini, S.; Wu, H.; Hill, A. H.; Manuel, P.; Attfield, J. P.; Argyriou, D. N.; Henry, P. F. *Physical Review Letters* **2012**, *108*, 217205.
(37) Belik, A. A.; Matsushita, Y.; Katsuya, Y.; Tanaka, M.; Kolodiazhnyi, T.; Isobe, M.; Takayama-Muromachi, E. *Physical Review B* **2011**, *84*, 6.
(38) Battle, P. D.; Gibb, T. C.; Jones, C. W. *Journal of Solid State Chemistry* **1988**, *74*, 60.
(39) Sondena, R.; Stolen, S.; Ravindran, P.; Grande, T.; Allan, N. L. *Physical Review B* **2007**, *75*, 184105.
(40) Fujii, K.; Shiraiwa, M.; Esaki, Y.; Yashima, M.; Kim, S. J.; Lee, S. *Journal of Materials Chemistry A* **2015**, *3*, 11985.
(41) Biegalski, M. D.; Haeni, J. H.; Trolier-McKinstry, S.; Schlom, D. G.; Brandle, C. D.; Graitis, A. J. V. *Journal of Materials Research* **2005**, *20*, 952.

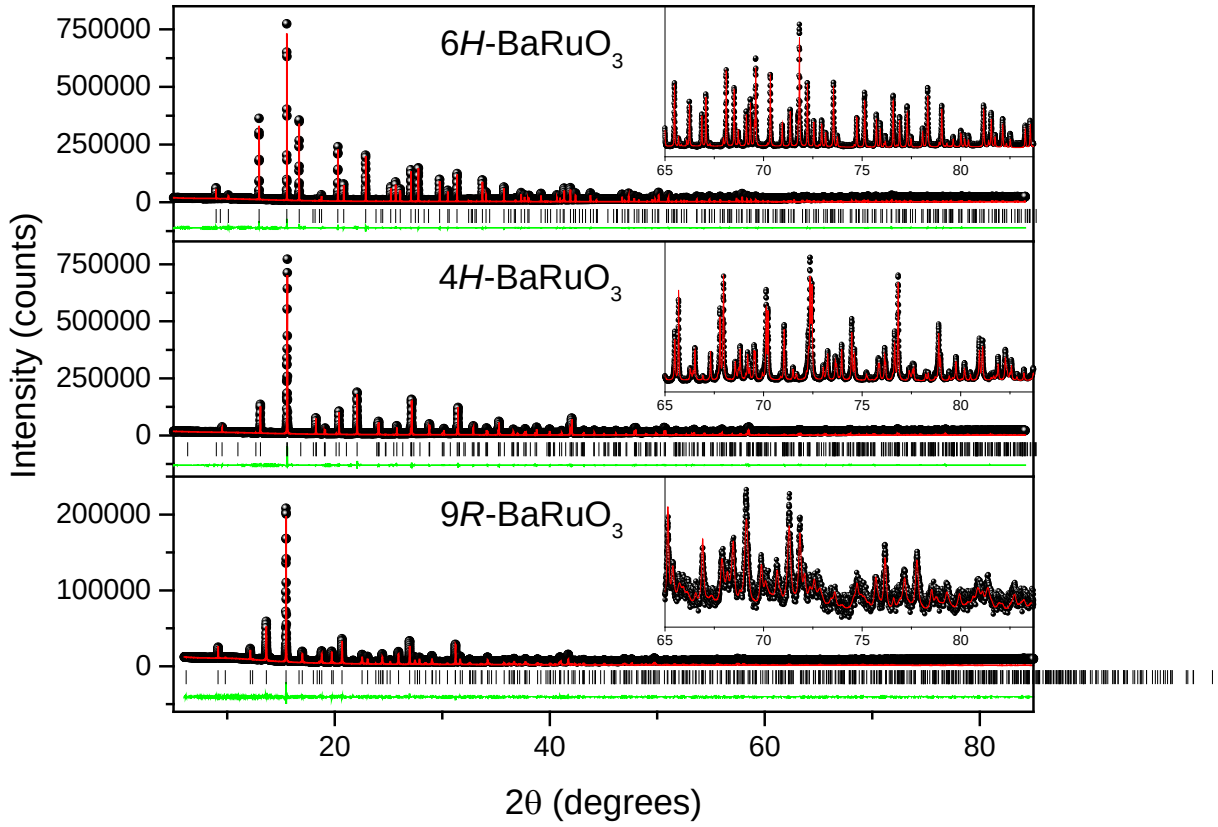

Figure 1: Rietveld fits to the Synchrotron X-ray diffraction data of $BaRuO_3$ at room temperature. The symbols are the observed data and the solid line joining them is the calculated profile. The lower solid line is the difference between the observed and calculated profiles and the positions of the space group allowed Bragg reflections are indicated by the vertical markers. The insets highlight the quality of the data and the fit to high angles.

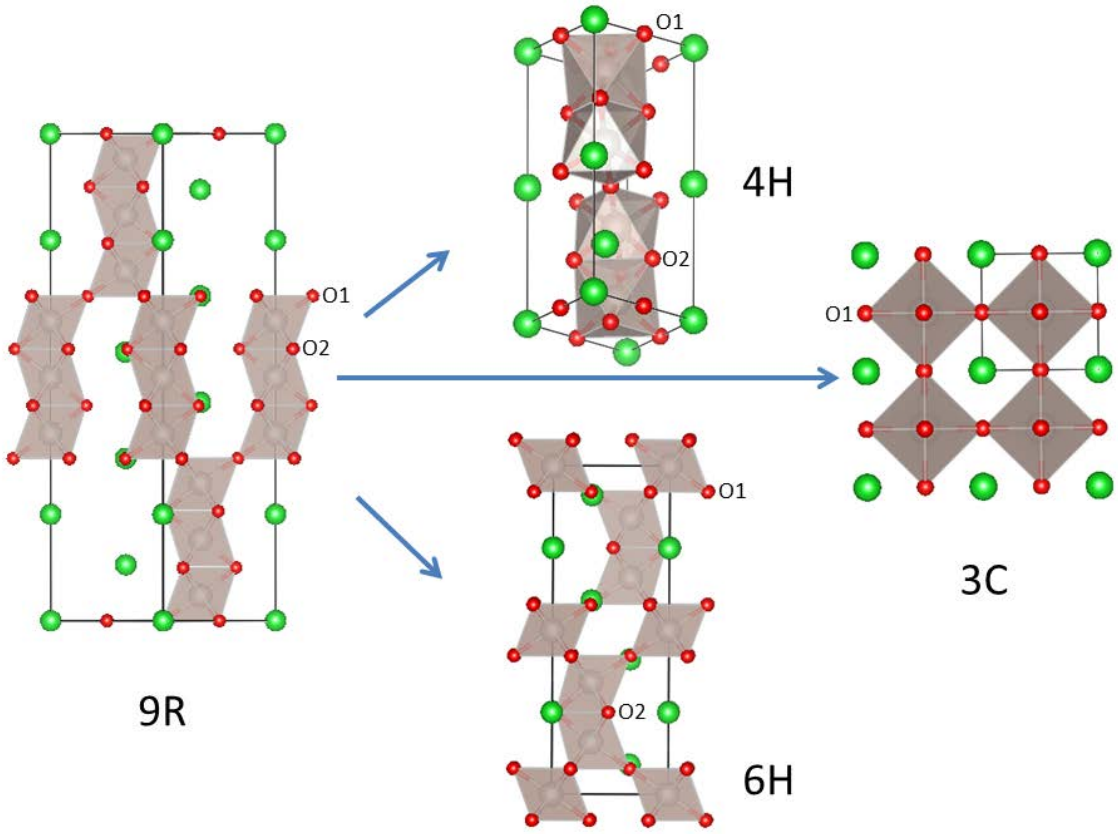

Figure 2. Representation of the four structures known for $BaRuO_3$. The larger spheres are the Ba cations and the smaller spheres represent the anions. In each of the structures the O(1) anions are corner sharing and the O(2) anions are face sharing. The Ru cations are at the centre of the octahedra.

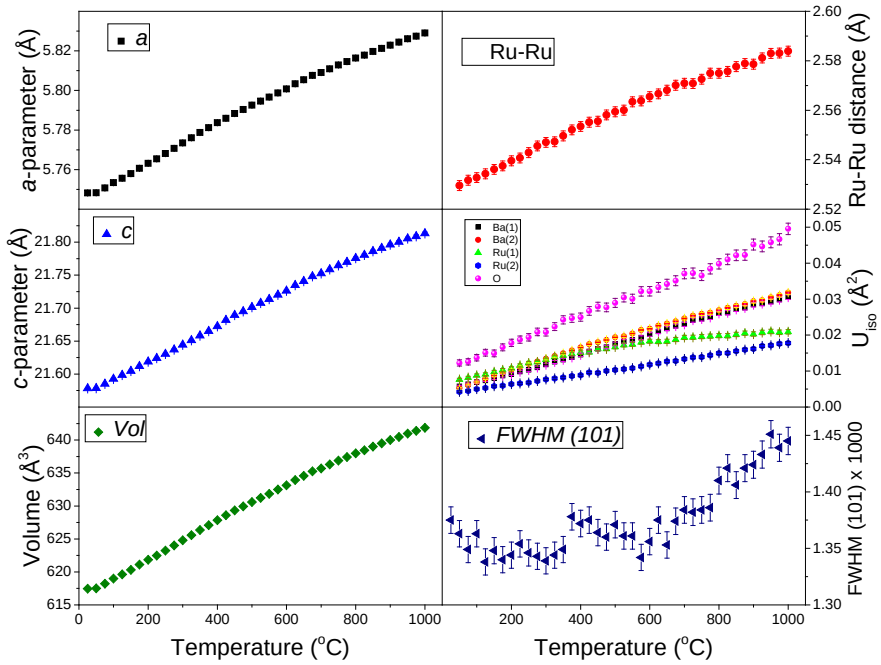

Figure 3: Thermal evolution of the lattice parameters, atomic displacement parameters and Ru-Ru distance in the 9*R*-$BaRuO_3$. Where not evident the estimated standard errors (esds) in the parameters are smaller than the symbols.

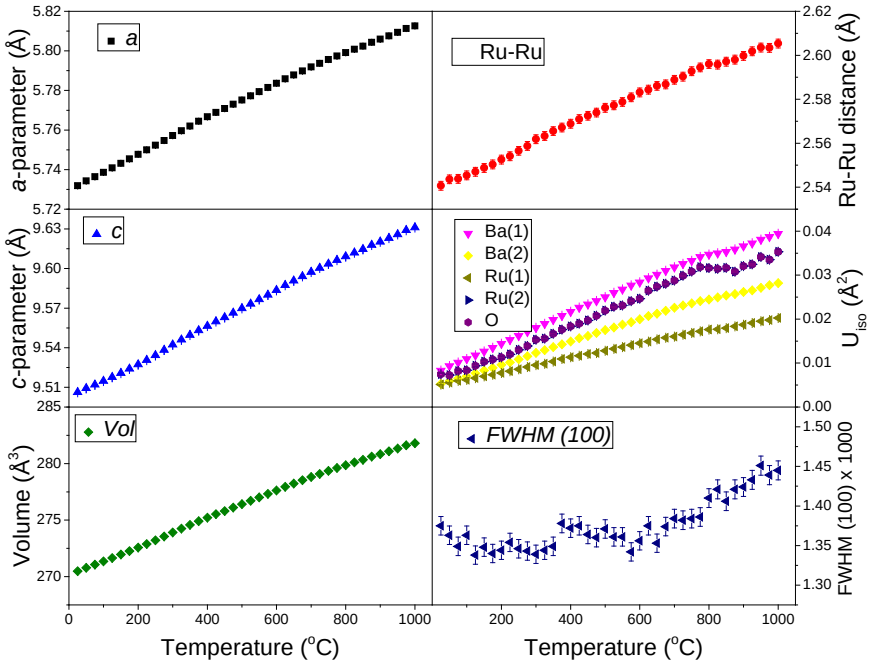

Figure 4: Thermal evolution of the lattice parameters, atomic displacement parameters and Ru-Ru distance in the 4*H* polymorph of $BaRuO_3$.

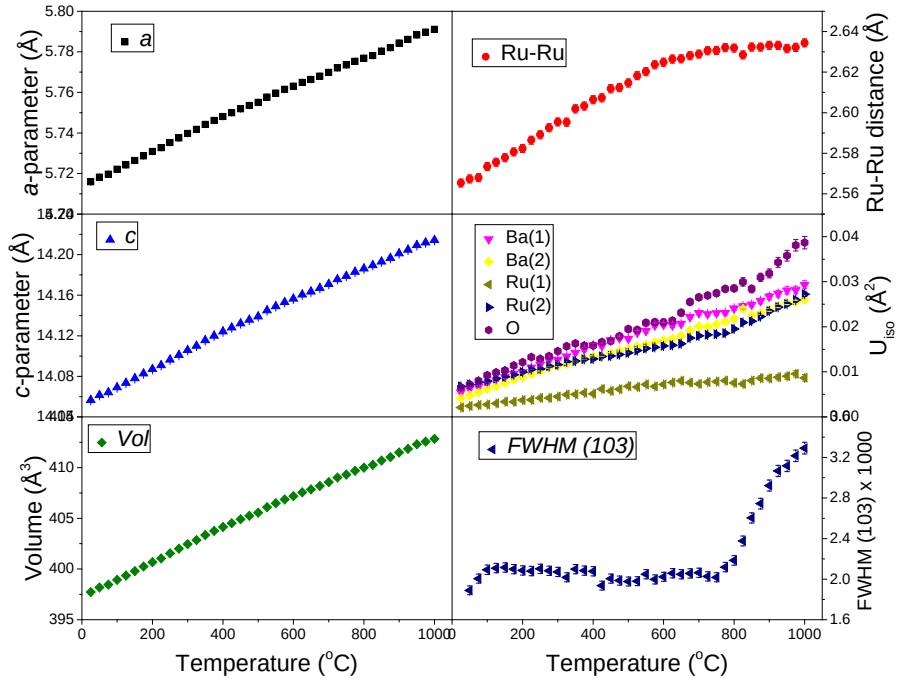

Figure 5: Thermal evolution of the lattice parameters, atomic displacement parameters and Ru-Ru distance in the 6*H* polymorph of $BaRuO_3$.

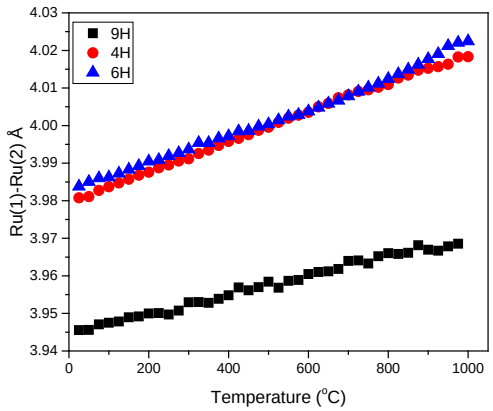

Figure 6. Temperature dependence of the Ru(1) – Ru(2) interatomic distances, across the shared corners in the 9*R*, 4*H* and 6*H* polymorphs of $BaRuO_3$.

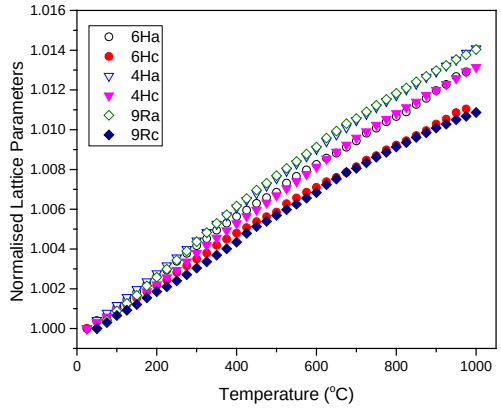

Figure 7. Normalised thermal expansion behaviour of the lattice parameters for the 9*R*, 4*H* and 6*H* polymorphs of $BaRuO_3$. The a-parameters are given as open symbols and the c-parameters as closed symbols

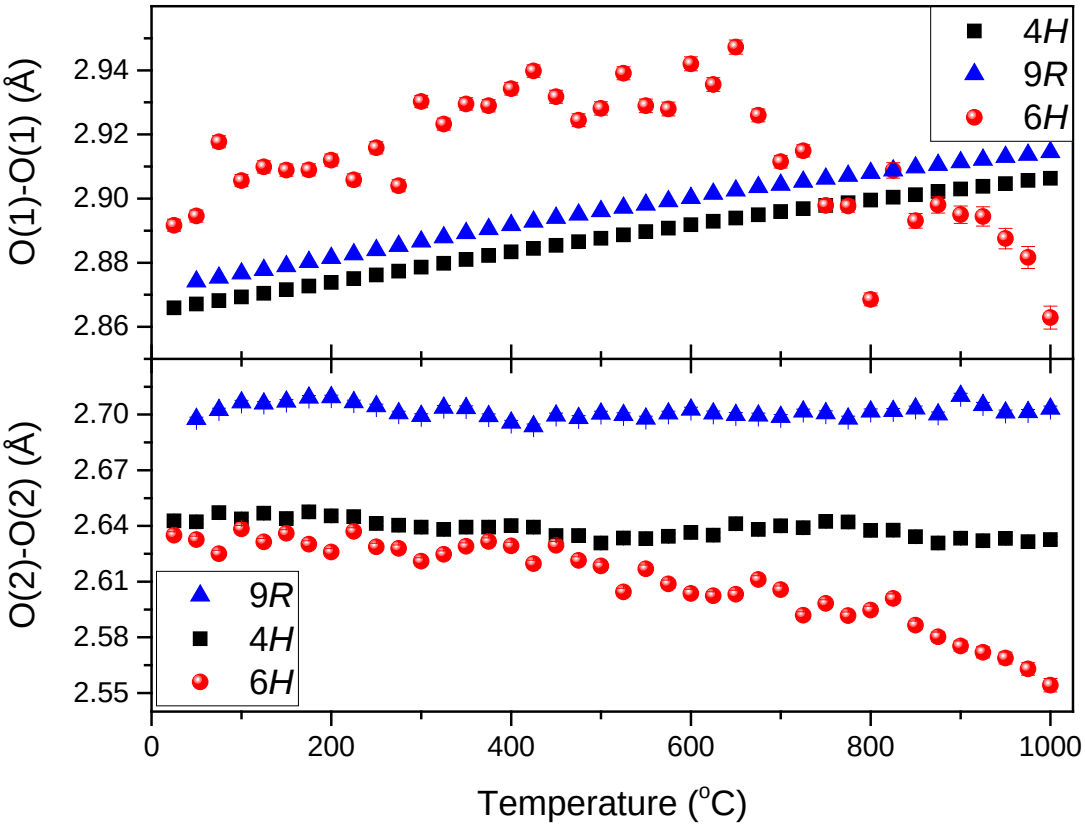

Figure 8: Temperature dependence of the O-O interatomic distances in the 9*R*, 4*H* and 6*H* polymorphs of $BaRuO_3$. Where not apparent the esds are smaller than the symbols.

Table 1 Unit Cell parameters, Atomic Coordinates and Atomic Displacement Parameters for the 9*R*, 4*H* and 6*H* polymorphs of $BaRuO_3$ at room temperature. The ADPs of the two anion sites were constrained to be equal. The Bond Valence Sums (BVS) for each ion are included.

	9*R*	4*H*	6*H*
Space Group	*R*3*m* No. 166	*P*6$_3$/*mmc* No. 194	*P*6$_3$/*mmc* No. 194
a Å	5.7482(2)	5.73187(2)	5.71590(6)
c Å	21.5783(8)	9.50625(3)	14.0566(2)
Vol Å^3	617.47(4)	270.478(2)	397.723(7)
R_p	0.036	0.030	0.038
R_{wp}	0.052	0.039	0.056
R_F^2	0.0491	0.0640	0.0665
χ^2	8.97	7.73	15.91
Ba(1) *x*, *y*, *z*	0, 0, 0	0, 0, 0	0, 0, ¼
U_{iso} x 100 (Å^2)	0.56(3)	0.830(7)	0.55(3)
BVS	2.32	2.19	2.46
Ba(2) *x*, *y*, *z*	0, 0, 0.21772(3)	1/3, 2/3, ¼	1/3 2/3 0.08998(4)
U_{iso} x 100 (Å^2)	0.48(2)	0.526(7)	0.412(12)
BVS	1.97	2.39	1.77
Ru(1) *x*, *y*, *z*	0, 0, ½	2/3, 1/3, 0.11637(4)	0, 0, 0
U_{iso} x 100 (Å^2)	0.79(3)	0.513(6)	0.21(3)
BVS	3.76	3.96	4.14
Ru(2) *x*, *y*, *z*	0, 0, 0.38308(5)	-	1/3, 2/3, 0.65875(4)
U_{iso} x 100 (Å^2)	0.33(2)	-	0.68(2)
BVS	3.95		3.86
O(1) *x*, *y*, *z*	½, 0, 0	½, ½, 0	0.5130(4), -*x*, ¼
U_{iso} x 100 (Å^2)	1.14(8)	0.744(28)	0.65(5)
BVS	2.06	2.11	2.17
O(2) *x*, *y*, *z*	0.1769(4), 2*x*, 0.1080(2)	0.3593(4), 2*x*, ¼	0.8353(5), -*x*, 0.0803(2)
U_{iso} x 100 (Å^2)	1.14(8)	0.74(3)	0.65(5)
BVS	2.01	2.02	2.11

Table 2 Selected interatomic distances (Å) in $BaRuO_3$ at room temperature.

	9*R*		4*H*		6*H*	
Ru(1)	O(2) x 6	2.007(4)	O(1) x 3	1.9907(2)	O(2) x 6	1.971
			O(2) x 3	1.9852(15)		
Ru(2)	O(1) x 3	1.9763(6)			O(1) x 3	1.981(3)
	O(2) x 3	2.001(4)			O(2) x 3	2.014(4)
Ba(1)	O(1) x 6	2.8741(1)	O(1) x 6	2.86594(1)	O(1) x 6	2.8612(2)
	O(2) x 6	2.914(4)	O(2) x 6	2.9716(12)	O(2) x 6	2.882(3)
Ba(2)	O(1) x 3	2.9960(6)	O(1) x 6	2.89603(1)	O(1) x 3	2.876(2)
	O(1) x 3	2.955(4)	O(2) x 6	2.86884(9)	O(2) x 6	2.8612(1)
	O(2) x 6	2.8809(3)			O(2) x 3	2.924(3)
Ru	Ru	2.523(1)	Ru	2.54067(7)	Ru	2.5626(11)
O(1)	O(1)	2.8741(2)	O(1)	2.8659(1)	O(1)	2.916(1)
O(2)	O(2)	2.698(3)	O(2)	2.642(4)	O(2)	2.616(4)

Table 3. Linear thermal expansion coefficients for $BaRuO_3$ between 50 and 600 °C

Polymorph	α_a (K^{-1})	α_c (K^{-1})	$\bar{\alpha}$ (K^{-1})
9*R*-$BaRuO_3$	16.4 x 10^{-6}	12.3 x 10^{-6}	15.1 x 10^{-6}
4*H*-$BaRuO_3$	15.7 x 10^{-6}	14.1 x 10^{-6}	15.2 x 10^{-6}
6*H*-$BaRuO_3$	14.4 x 10^{-6}	12.3 x 10^{-6}	13.7 x 10^{-6}